



# Characteristics of phase bias from CNES and its application in multi-frequency and multi-GNSS precise point positioning with ambiguity resolution

Tianjun Liu<sup>1</sup> · Hua Chen<sup>2</sup> · Qusen Chen<sup>1</sup> · Weiping Jiang<sup>1</sup> · Denis Laurichesse<sup>3</sup> · Xiangdong An<sup>1</sup> · Tao Geng<sup>1</sup>

Received: 30 August 2020 / Accepted: 24 January 2021 / Published online: 12 February 2021  
© The Author(s), under exclusive licence to Springer-Verlag GmbH, DE part of Springer Nature 2021

## Abstract

While precise point positioning ambiguity resolution (PPP AR) is a valuable tool of the multi-constellation global navigation satellite system (multi-GNSS), phase biases are critical to implement PPP AR. Multi-frequency phase biases and satellite attitude files are provided freely by Centre National d'Etudes Spatiales (CNES), which are estimated based on GeoForschungs Zentrum (GFZ) satellite rapid orbit and clock products. However, the temporal characteristics of these phase biases and their positioning performance in the multi-frequency and multi-GNSS PPP AR have not been investigated yet, especially in the low sun elevation and satellite maneuver period. We introduce the transformation between multi-frequency phase biases and integer recovery clock model. In this transformation, inter-frequency clock biases (IFCBs) and inconsistencies in satellite attitude model errors between GFZ and CNES products are well considered. Experiments with GPS/Galileo/BeiDou observations from 34 stations were performed in static and kinematic modes, and the multi-frequency phase residuals were analyzed in the low sun elevation. Our results show that the impact of IFCBs and inconsistencies in satellite attitude errors could be mitigated at the user ends by using phase biases and satellite attitude files. Under the condition of satellite reverse yaw maneuvers, the performance of kinematic PPP without phase biases or deleting maneuvering satellites would be degraded significantly until the end of satellite observation arc or the next reverse yaw maneuver occurs. By applying phase biases with PPP AR, the positioning accuracy could be improved by 34.4%, 23.1%, and 37.4% in the east (E), north (N), and up (U) directions, respectively. Therefore, we suggested that PPP users should apply phase biases and satellite attitude files when using the GFZ rapid orbit and clock products, especially for satellite maneuvers and low sun elevation.

**Keywords** Multi-frequency and multi-GNSS · Reverse yaw maneuvers · Satellite attitude · Inter-frequency clock bias · Ambiguity resolution

## Introduction

Precise point positioning (PPP) is an absolute positioning technology for global navigation satellite system (GNSS) and is widely used in scientific research and civilian applications (Malys and Jensen 1990; Zumberge et al. 1997;

Kouba and Héroux 2001; Montenbruck et al. 2017). Since its development, PPP and its applications quickly became a hot topic in the GNSS community and developed into one of the most representative technologies in GNSS precise positioning. However, there are still some unresolved difficulties in high-precision PPP applications, such as multi-frequency and multi-GNSS PPP with successful ambiguity resolution (AR), inconsistencies in the satellite attitude model between network and user ends, together with the inter-frequency clock bias (IFCBs) of the GPS L5 signal in multi-frequency PPP.

With the rapid development and modernization of GNSS, its users can benefit from multi-frequency and multi-GNSS satellites, such as carrier phase multipath extraction, cycle slip processing, high-order ionosphere mitigation, and efficient AR in particular (Zhang and Li 2016; Li et al. 2018,

✉ Qusen Chen  
chenqs@whu.edu.cn

<sup>1</sup> GNSS Research Center, Wuhan University, 129 Luoyu Road, Wuhan 430079, China

<sup>2</sup> School of Geodesy and Geomatics, Wuhan University, 129 Luoyu Road, Wuhan 430079, China

<sup>3</sup> Centre National D'Etudes Spatiales, 14 avenue Edouard Belin, 31400 Toulouse, France

2019; Zhou et al 2019). A higher PPP performance can be achieved with AR than ambiguity-float PPP (Laurichesse et al. 2009; Ge et al. 2008; Collins et al. 2008). Traditionally, PPP AR can be achieved by adopting integer recovery clocks (IRCs) or uncalibrated phase delays (UPDs), which are estimated by using dual-frequency ionosphere-free (IF) combination observations through reference network and then issued to PPP users. The corresponding relationship and equivalence of these two methods are investigated and proved by Geng et al. (2010) as well as Shi and Gao (2014). Unfortunately, unlike the classic dual-frequency model, IFCBs exist between GPS L1/L2 and L1/L5 IF observations, which are primarily caused by large variations in the GPS L5 phase hardware delay (Montenbruck et al. 2012). The existence of such pronounced IFCBs makes it impossible or inappropriate to use one set of satellite clock products in data processing for all frequencies (Guo and Geng 2018; Pan et al. 2017).

On the other hand, to obtain more accurate PPP solutions, the consistency of satellite attitude models between network and user ends must be ensured. During satellites maneuver periods, how to accurately model the non-nominal yaw attitudes and eliminate their effect is of particular interest to many researchers (Kouba 2009; Dilssner et al. 2011; Wang et al. 2018; Montenbruck et al. 2017). The impact of satellite reverse yaw maneuvers on BeiDou precise orbit determination (POD) has been assessed, and phase residuals of nearly 40 cm can be caused with the yaw attitude model previously established by Wuhan University (Xia et al. 2019). International GNSS Service (IGS) Analysis Centers (ACs) employ various strategies in non-nominal yaw attitude treatment. However, most of the PPP users are not concerned with how these orbit and clock products are generated and directly use them, which causes centimeter-level errors in the kinematic PPP solutions, since an inconsistent attitude model is applied with respect to the ACs (Lou et al. 2015; Loyer et al. 2017). Therefore, to ensure consistency between network and user ends is a critical issue for reducing positioning errors. Because of this reason, exchanging satellite attitude information in the ORBit EXchange (ORBEX) format among ACs is being tested (Banville et al. 2020; Loyer et al. 2017).

To address the above issues and be compatible with multi-frequency PPP AR, a new phase bias model compatible with Bias Solution INdependent EXchange Format (Bias-SINEX) format has been presented by Centre National d’Etudes Spatiales (CNES) (Laurichesse and Privat 2015; Schaer 2016). The post-processed phase biases, which are estimated based on the GeoForschungs Zentrum (GFZ) satellites rapid orbit and clock products, are saved as files available on the CNES website ([www.ppp-wizard.net/products/POST\\_PROCESSED](http://www.ppp-wizard.net/products/POST_PROCESSED)). Considering the inconsistency of satellite attitude model between CNES and GFZ, satellite attitude files with attitude quaternions of GNSS satellites are provided by CNES. Nevertheless, only initial studies on these phase biases have

been given by Banville et al. (2020) and Liu et al. (2020). In their research, the performance of the dual-frequency PPP model was studied, but ambiguity fixing should be extended with more than dual frequencies. Moreover, the impact of GPS L5 IFCBs and attitude model inconsistency errors are rarely investigated by using these phase biases, especially in the conditions of satellite maneuvers and low sun elevation. Hence, we believe that it is still necessary to carry out a detailed and deep research on these topics to better understand the characteristics of phase biases and their application in multi-GNSS and multi-frequency PPP AR.

By using a modified version of the Precise Point Positioning with Integer and Zero-difference Ambiguity Resolution Demonstrator (PPP-WIZARD, Laurichesse and Privat 2015), the temporal characteristics of post-processed phase biases are assessed, and the position performance is evaluated in static, kinematic PPP AR. Following the introduction, the undifferenced and uncombined GPS/Galileo/BeiDou multi-frequency PPP observation model is presented through applying GFZ rapid orbit, clock products, and CNES satellite attitude files. We then introduce the transformation between phase biases and IRC model in the case of multi-frequency. Meanwhile, the reason GPS L5 IFCBs and satellite attitude model inconsistency errors can be absorbed into phase biases is also explained. Furthermore, the impact of phase biases on the carrier phase residual for multi-frequency PPP is analyzed in low sun elevation and satellite maneuver periods, and the positioning accuracy is assessed during the reverse yaw maneuver period. Finally, conclusions and perspectives are summarized.

### Multi-frequency and multi-GNSS PPP model

With GFZ rapid clock, orbit products, and CNES satellite attitude files, the raw observation equations of multi-frequency GNSS PPP for code  $P$  and carrier phase  $L$  observations at a particular epoch can be expressed as follows:

$$P_{r,i}^{sys,s} = D_{r,i}^{sys,s} + c(dt_r^{sys} - dt_{GFZ}^{sys,s}) + \gamma_i^{sys} \cdot I_1^{sys,s} + T_r + b_{r,P}^{sys} - b_{P_i}^{sys,s} + yaw_{i,CNES-GFZ}^{sys,s} \tag{1}$$

$$\lambda_i^{sys} L_{r,i}^{sys,s} = D_{r,i}^{sys,s} + c(dt_r^{sys} - dt_{GFZ}^{sys,s}) - \gamma_i^{sys} \cdot I_1^{sys,s} + T_r + \lambda_i^{sys} \cdot (N_{r,i}^{sys,s} + b_{r,L_i}^{sys} - b_{L_i}^{sys,s}) + yaw_{i,CNES-GFZ}^{sys,s} + \epsilon_{r,i}^s \tag{2}$$

where  $i = 1, 2, 3, 4$  refers to the carrier frequency;  $s$  and  $r$  denote the satellite and receiver, respectively;  $sys$  denotes different satellite systems, which could be G (GPS), E (Galileo), or C (BeiDou);  $\lambda_i^{sys}$  denotes the wavelength of carrier

phase observations at frequency  $f_i^{sys}$ , and  $D_{r,i}^{sys,s}$  is the geometric distance between satellite and receiver antennas.  $dt_{GFZ}^{sys,s}$  and  $dt_r^{sys}$  are the GFZ satellite code clock (satellite code clock is available from the IGS convention) and receiver clock, respectively;  $c$  is the speed of light in vacuum;  $I_1^{sys,s}$  represents the slant ionospheric delay at the first frequency  $f_1^{sys}$ ;  $\gamma_i^{sys} = (f_1^{sys}/f_i^{sys})^2$  is a corresponding coefficient;  $T_r$  is the slant tropospheric delay;  $N_i^s$  denotes the integer ambiguity for each frequency.  $b_{r,P_i}^{sys}$  and  $b_{r,L_i}^{sys}$  are the receiver code and phase hardware delay, respectively.  $b_{P_i}^{sys,s}$  and  $b_{L_i}^{sys,s}$  are the satellite code and phase hardware delay, respectively. The variation in the GPS L5 phase hardware delay is large at low sun elevation (Montenbruck et al. 2012; Pan et al. 2017); hence, the GPS L5 satellite phase hardware delay  $b_{L_5}^{G,s} + \delta b_{L_5}^{G,s}$  should be divided into time-invariant parts  $b_{L_5}^{G,s}$  and time-dependent parts  $\delta b_{L_5}^{G,s}$ . Since the satellite attitude files from CNES are used, to obtain more higher accuracy, the yaw attitude errors  $yaw_{i,CNES-GFZ}$  (such as phase center offsets (PCO) and phase wind-up) caused by inconsistent satellite attitude model between the GFZ and CNES must be considered (Loyer et al. 2017; Lou et al. 2015). The CNES provided satellite attitude is presented in the form of four quaternion elements  $(q_0, q_1, q_2, q_3)$ , and the unit vectors  $(e_x, e_y, e_z)$  in the satellite-fixed coordinate system can be defined as (Loyer et al. 2017):

$$\begin{aligned}
 e_x &= \begin{bmatrix} q_0^2 + q_1^2 - q_2^2 - q_3^2 \\ 2 \cdot (q_1 q_2 - q_0 q_3) \\ 2 \cdot (q_1 q_3 + q_0 q_2) \end{bmatrix} \\
 e_y &= \begin{bmatrix} 2 \cdot (q_1 q_2 + q_0 q_3) \\ q_0^2 - q_1^2 + q_2^2 - q_3^2 \\ 2 \cdot (q_2 q_3 - q_0 q_1) \end{bmatrix} \\
 e_z &= \begin{bmatrix} 2 \cdot (q_1 q_3 - q_0 q_2) \\ 2 \cdot (q_2 q_3 + q_0 q_1) \\ q_0^2 - q_1^2 - q_2^2 + q_3^2 \end{bmatrix}
 \end{aligned} \tag{3}$$

If rapid satellite orbit and clock products from GFZ are applied in the multi-frequency undifferenced and uncombined observation equations (Liu et al. 2020), the GPS-only ( $sys = G$ ) narrow-lane  $\bar{N}_1^s$ , wide-lane (WL)  $\bar{N}_W^s$ , and extra-wide-lane (EWL)  $\bar{N}_E^s$  ambiguities can be formulated as:

$$\begin{cases}
 \lambda_1 \cdot \bar{N}_1^s &= \lambda_1 \cdot (N_1^s + b_{r,L_1} - b_{L_1}^s) + b_{P_{IF}}^s - b_{r,P_{IF}} + \beta_{12} (DCB_{r,12} + DCB_{12}^s) \\
 \lambda_2 \cdot (\bar{N}_W^s + \bar{N}_1^s) &= \lambda_2 \cdot (N_2^s + b_{r,L_2} - b_{L_2}^s) + b_{P_{IF}}^s - b_{r,P_{IF}} + \gamma_2 \beta_{12} (DCB_{r,12} + DCB_{12}^s) \\
 \lambda_5 \cdot (\bar{N}_E^s + \bar{N}_W^s + \bar{N}_1^s) &= \lambda_5 \cdot (N_5^s + b_{r,L_5} - b_{L_5}^s) + b_{P_{IF}}^s - b_{r,P_{IF}} + \gamma_5 \beta_{12} (DCB_{r,12} + DCB_{12}^s) \\
 DCB_{r,12} &= b_{r,P_1} - b_{r,P_2} \quad DCB_{12}^s = b_{P_1}^s - b_{P_2}^s \\
 b_{P_{IF}}^s &= \alpha_{12} \cdot b_{P_1}^s + \beta_{12} \cdot b_{P_2}^s \quad b_{r,P_{IF}} = \alpha_{12} \cdot b_{r,P_1} + \beta_{12} \cdot b_{r,P_2} \\
 \alpha_{12} &= f_1^2 / (f_1^2 - f_2^2) \quad \beta_{12} = -f_2^2 / (f_1^2 - f_2^2)
 \end{cases} \tag{4}$$

where  $DCB_{12}^s$  and  $DCB_{r,12}$  denote the difference code biases at satellite  $s$  and receiver  $r$ , respectively. Since satellite and receiver hardware delays are highly correlated with integer ambiguity, the integer property of the estimated ambiguity parameter  $\bar{N}_1^s, \bar{N}_W^s, \bar{N}_E^s$  will be lost. Note that time-dependent parts  $\delta b_{L_5}^{G,s}$  of the GPS L5 phase hardware delays are not compensated by the precise code satellite clocks  $dt_{GFZ}^s$ , which are estimated based on dual-frequency (L1 and L2) measurement observations, and these time-dependent parts  $\delta b_{L_5}^{G,s}$  will have an influence on the GPS L5 phase residuals (Cao et al. 2018). Moreover, due to the mixed application of GFZ rapid orbit, clock products, and CNES yaw attitude model, the inconsistent yaw attitude errors  $yaw_{i,CNES-GFZ}$  will also cause systematic errors during satellite maneuver period (Lou et al. 2015; Loyer et al. 2017; Kouba 2009). Finally, the phase residuals symbolized as  $v_{L_i}^s$  in each GPS frequency can be expressed as follows:

$$\begin{bmatrix} v_{L_1}^{G,s} \\ v_{L_2}^{G,s} \\ v_{L_5}^{G,s} \end{bmatrix} = \begin{bmatrix} \epsilon_{r,1}^{G,s} + yaw_{1,CNES-GFZ}^G \\ \epsilon_{r,2}^{G,s} + yaw_{2,CNES-GFZ}^G \\ \epsilon_{r,5}^{G,s} + yaw_{5,CNES-GFZ}^G + \delta b_{L_5}^{G,s} \end{bmatrix} \tag{5}$$

while for Galileo and BeiDou system ( $sys = E, C$ ), phase residuals can be expressed as follows:

$$\begin{bmatrix} v_{L_1}^{E,s} \\ v_{L_5}^{E,s} \\ v_{L_7}^{E,s} \\ v_{L_6}^{E,s} \end{bmatrix} = \begin{bmatrix} \epsilon_{r,1}^{E,s} + yaw_{1,CNES-GFZ}^{E,s} \\ \epsilon_{r,5}^{E,s} + yaw_{5,CNES-GFZ}^{E,s} \\ \epsilon_{r,7}^{E,s} + yaw_{7,CNES-GFZ}^{E,s} \\ \epsilon_{r,6}^{E,s} + yaw_{6,CNES-GFZ}^{E,s} \end{bmatrix}$$

$$\begin{bmatrix} v_{L_2}^{C,s} \\ v_{L_7}^{C,s} \\ v_{L_6}^{C,s} \end{bmatrix} = \begin{bmatrix} \epsilon_{r,2}^{C,s} + yaw_{2,CNES-GFZ}^{C,s} \\ \epsilon_{r,7}^{C,s} + yaw_{7,CNES-GFZ}^{C,s} \\ \epsilon_{r,6}^{C,s} + yaw_{6,CNES-GFZ}^{C,s} \end{bmatrix} \tag{6}$$

Due to the smaller effect of time-dependent parts on Galileo E5b, E6 and BeiDou B3 phase hardware delays with the current GFZ rapid products (Cao et al. 2018; Li et al. 2018), these errors will not be considered for the multi-frequency and multi-GNSS PPP model in this study.

### Transformation between the phase bias and IRC model for multi-frequency PPP

AR at the PPP user end can be implemented by applying the IRC model (Laurichesse et al. 2009). Different from the IRC model, PPP user end can use phase biases and code satellite clocks to recover the integer properties of ambiguities. Taking GPS as an example, the phase biases  $\bar{b}_{L_i}^s$  are estimated by using the integer phase clock  $dt_{IRC}^s$ , code satellite clock  $dt_{GFZ}^s$ , and triple-frequency IF phase combination  $L_{IF_3}$  (Liu et al. 2020). The precise code satellite clocks  $dt_{GFZ}^s$  can be obtained with dual-frequency IF phase combination:

$$cdt_{GFZ}^s = cdt^s + b_{P_{IF}}^s = cdt^s + \frac{\gamma_2 \cdot b_{P_1}^s - b_{P_2}^s}{(\gamma_2 - 1)} \tag{7}$$

Based on the GFZ rapid orbit products and CNES satellite yaw attitude model, the inconsistent yaw attitude error  $yaw_{i,CNES-GFZ}$  will be absorbed into integer phase clocks  $dt_{IRC}^s$  during the satellite maneuver period (Lou et al. 2015; Loyer et al. 2017). Therefore, the integer phase clocks  $dt_{IRC}^s$  can be presented as follows:

$$cdt_{IRC}^s = cdt^s + \frac{\gamma_2 \cdot \lambda_1 \cdot b_{L_1}^s - \lambda_2 \cdot b_{L_2}^s}{(\gamma_2 - 1)} + \frac{\gamma_2 \cdot yaw_{1,CNES-GFZ}^s - yaw_{2,CNES-GFZ}^s}{(\gamma_2 - 1)} \tag{8}$$

To make multi-frequency phase biases  $\bar{b}_{L_i}^s$  compatible with code satellite clocks  $dt_{GFZ}^s$ , the difference  $cdt_{IRC}^s - cdt_{GFZ}^s$  should be assimilated into phase biases  $\bar{b}_{L_i}^s$ . Combining (7) and (8), the estimated phase biases  $\bar{b}_{L_1}^s, \bar{b}_{L_2}^s$  can be determined by  $cdt_{IRC}^s - cdt_{GFZ}^s$ :

$$\frac{\gamma_2 \cdot \lambda_1 \cdot \bar{b}_{L_1}^s - \lambda_2 \cdot \bar{b}_{L_2}^s}{(\gamma_2 - 1)} = cdt_{IRC}^s - cdt_{GFZ}^s \tag{9}$$

The phase biases  $\bar{b}_{L_i}^s$  for each frequency cannot be resolved due to rank deficiency of (9). In the multi-frequency case, using GFZ rapid orbit, clock products and the CNES satellite yaw attitude model, the phase bias difference among  $\bar{b}_{L_1}^s, \bar{b}_{L_2}^s, \bar{b}_{L_5}^s$  can be obtained by applying triple-frequency IF phase combination  $L_{IF_3}$  (Liu et al. 2020):

$$L_{IF_3} = \frac{f_1 \cdot \lambda_{WL_{L1L2}} \cdot (L_1 - L_2)}{f_1 - f_5} - \frac{f_5 \cdot \lambda_{WL_{L2L5}} \cdot (L_2 - L_5)}{f_1 - f_5} = D_r^s + T_r + \bar{dt}_r - cdt_{GFZ}^s + \frac{f_1 \cdot \lambda_{WL_{L1L2}} \cdot \bar{N}_W^s}{f_1 - f_5} - \frac{f_5 \cdot \lambda_{WL_{L2L5}} \cdot \bar{N}_E^s}{f_1 - f_5} \tag{10}$$

with

$$\lambda_{WL_{L1L2}} = \frac{c}{f_1 - f_2} \quad \lambda_{WL_{L2L5}} = \frac{c}{f_2 - f_5} \tag{11}$$

where  $\lambda_{WL_{L1L2}}$  and  $\lambda_{WL_{L2L5}}$  are the WL and EWL wavelengths, respectively. In Eq. (10), WL ambiguities can be obtained from IRC model,  $D_r^s$  and  $cdt_{GFZ}^s$  are fixed, while  $\bar{N}_E^s, \bar{N}_W^s$  are estimated as completely independent between epochs. Therefore, the GPS L5 time-dependent parts  $\delta b_{L_5}^{G,s}$  and yaw attitude error  $yaw_{i,CNES-GFZ}$  will be absorbed into  $\bar{N}_W^s, \bar{N}_E^s$ :

$$\begin{aligned} \bar{N}_W^s &= N_W^s + \frac{\gamma_2 \cdot b_{P_1}^s - b_{P_2}^s}{(\gamma_2 - 1)\lambda_{WL_{L1L2}}} - \frac{yaw_{1,CNES-GFZ}^s}{\lambda_1} \\ &\quad + \frac{yaw_{2,CNES-GFZ}^s}{\lambda_2} - b_{L_1}^s + b_{L_2}^s \\ \bar{N}_E^s &= N_E^s + \frac{\gamma_2 \cdot b_{P_1}^s - b_{P_2}^s}{(\gamma_2 - 1)\lambda_{WL_{L2L5}}} - \frac{yaw_{2,CNES-GFZ}^s}{\lambda_2} \\ &\quad + \frac{yaw_{5,CNES-GFZ}^s}{\lambda_5} - b_{L_2}^s + b_{L_5}^s + \delta b_{L_5}^{G,s} \end{aligned} \tag{12}$$

The phase bias difference among  $\bar{b}_{L_1}^s, \bar{b}_{L_2}^s, \bar{b}_{L_5}^s$  can then be expressed as fractional parts of  $\bar{N}_W^s$  and  $\bar{N}_E^s$ :

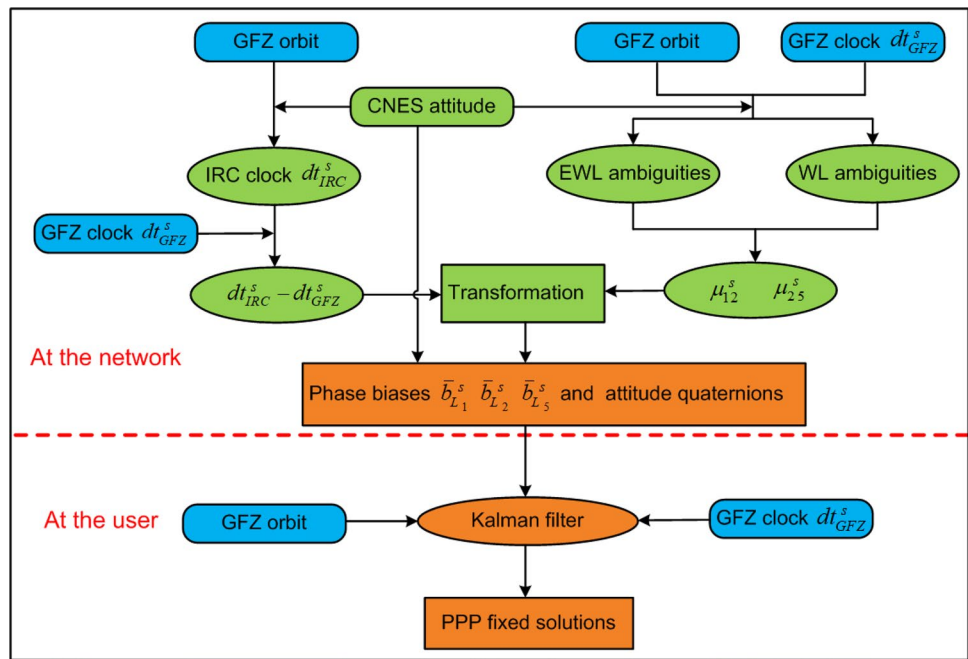
$$\begin{aligned} \mu_{12}^s &= \bar{b}_{L_1}^s - \bar{b}_{L_2}^s = \bar{N}_W^s - \langle \bar{N}_W^s \rangle \\ &= \frac{\gamma_2 \cdot b_{P_1}^s - b_{P_2}^s}{(\gamma_2 - 1)\lambda_{WL_{L1L2}}} - \frac{yaw_{1,CNES-GFZ}^s}{\lambda_1} \\ &\quad + \frac{yaw_{2,CNES-GFZ}^s}{\lambda_2} - b_{L_1}^s + b_{L_2}^s \\ \mu_{25}^s &= \bar{b}_{L_2}^s - \bar{b}_{L_5}^s = \bar{N}_E^s - \langle \bar{N}_E^s \rangle \\ &= \frac{\gamma_2 \cdot b_{P_1}^s - b_{P_2}^s}{(\gamma_2 - 1)\lambda_{WL_{L2L5}}} - \frac{yaw_{2,CNES-GFZ}^s}{\lambda_2} \\ &\quad + \frac{yaw_{5,CNES-GFZ}^s}{\lambda_5} - b_{L_2}^s + b_{L_5}^s + \delta b_{L_5}^{G,s} \end{aligned} \tag{13}$$

where  $\langle * \rangle$  means to round the real value to the nearest integer value and  $\mu_{12}^s, \mu_{25}^s$  are the fractional parts of  $\bar{N}_W^s, \bar{N}_E^s$ . Combining (9) and (13), the estimated phase bias parameters  $\bar{b}_{L_1}^s, \bar{b}_{L_2}^s, \bar{b}_{L_5}^s$  can be determined with the 3\*3 matrix in the triple-frequency case:

$$\begin{pmatrix} \bar{b}_{L_1}^s \\ \bar{b}_{L_2}^s \\ \bar{b}_{L_5}^s \end{pmatrix} = \frac{1}{\gamma_2 \lambda_1 - \lambda_2} \begin{pmatrix} -\lambda_2 & 1 & 0 \\ -\gamma_2 \lambda_1 & 1 & 0 \\ -\gamma_2 \lambda_1 & 1 & -1 \end{pmatrix} \cdot \begin{pmatrix} \mu_{12}^s \\ (\gamma_2 - 1)(cdt_{IRC}^s - cdt_{IGS}^s) \\ \mu_{25}^s \end{pmatrix} \tag{14}$$

among which  $\mu_{12}^s, \mu_{25}^s, cdt_{IRC}^s, cdt_{GFZ}^s$  are represented by  $b_{P_{IF}}^s, b_{L_i}^s, yaw_{i,CNES-GFZ}^s$ , so that we can simplify the above transformation as:

**Fig. 1** Estimation of phase biases in the multi-frequency case



$$\begin{pmatrix} \bar{b}_{L_1}^s \\ \bar{b}_{L_2}^s \\ \bar{b}_{L_5}^s \end{pmatrix} = \begin{pmatrix} \frac{1}{\lambda_1} \cdot b_{P_{IF}}^s - b_{L_1}^s - \frac{1}{\lambda_1} \cdot yaw_{1,CNES-GFZ}^s \\ \frac{1}{\lambda_2} \cdot b_{P_{IF}}^s - b_{L_2}^s - \frac{1}{\lambda_2} \cdot yaw_{2,CNES-GFZ}^s \\ \frac{1}{\lambda_5} \cdot b_{P_{IF}}^s - b_{L_5}^s - \frac{1}{\lambda_5} \cdot yaw_{5,CNES-GFZ}^s - \delta b_{L_5}^{G,s} \end{pmatrix} \tag{15}$$

This transformation can be described in Fig. 1:

Considering that the code biases  $\bar{b}_{P_i}^s$  are standardized in Bias-SINEX format V1.00 (Schaer 2016; Banville et al. 2020), these biases can be expressed as follows:

$$\begin{pmatrix} \bar{b}_{P_1}^s \\ \bar{b}_{P_2}^s \\ \bar{b}_{P_5}^s \end{pmatrix} = \begin{pmatrix} \beta_{12} (b_{P_1}^s - b_{P_2}^s) \\ -\alpha_{12} (b_{P_1}^s - b_{P_2}^s) \\ b_{P_{IF}}^s - b_{P_5}^s \end{pmatrix} \tag{16}$$

The PPP user end applies code and phase biases to raw measurements with the GFZ code satellite clock  $dt_{GFZ}^s$  and CNES satellite attitude, the integer properties of ambiguities can then be recovered, GPS L5 IFCBs and yaw-attitude errors  $yaw_{i,CNES-GFZ}$  can also be mitigated at the PPP user end. The reparameterization of (4) for GPS, as an example, can be conducted as:

$$\begin{cases} \lambda_1 \cdot \bar{N}_1^s & = \lambda_1 \cdot (N_1^s + b_{r,L_1}) - b_{r,P_{IF}} + \beta_{12} DCB_{r,12} \\ \lambda_2 \cdot (\bar{N}_W + \bar{N}_1^s) & = \lambda_2 \cdot (N_2^s + b_{r,L_2}) - b_{r,P_{IF}} + \gamma_2 \beta_{12} DCB_{r,12} \\ \lambda_5 \cdot (\bar{N}_E + \bar{N}_W + \bar{N}_1^s) & = \lambda_5 \cdot (N_5^s + b_{r,L_5}) - b_{r,P_{IF}} + \gamma_5 \beta_{12} DCB_{r,12} \end{cases} \tag{17}$$

The carrier phase residual errors  $v_{L_i}^s$  in the multi-frequency case can be expressed as follows:

$$\begin{bmatrix} v_{L_1}^{G,s} \\ v_{L_2}^{G,s} \\ v_{L_5}^{G,s} \end{bmatrix} = \begin{bmatrix} \epsilon_{r,1}^{G,s} \\ \epsilon_{r,2}^{G,s} \\ \epsilon_{r,5}^{G,s} \end{bmatrix} \quad \begin{bmatrix} v_{L_1}^{E,s} \\ v_{L_5}^{E,s} \\ v_{L_7}^{E,s} \\ v_{L_6}^{E,s} \end{bmatrix} = \begin{bmatrix} \epsilon_{r,1}^{E,s} \\ \epsilon_{r,5}^{E,s} \\ \epsilon_{r,7}^{E,s} \\ \epsilon_{r,6}^{E,s} \end{bmatrix} \tag{18}$$

$$\begin{bmatrix} v_{L_2}^{C,s} \\ v_{L_7}^{C,s} \\ v_{L_6}^{C,s} \end{bmatrix} = \begin{bmatrix} \epsilon_{r,2}^{C,s} \\ \epsilon_{r,7}^{C,s} \\ \epsilon_{r,6}^{C,s} \end{bmatrix}$$

These post-processed GPS/Galileo/BeiDou multi-frequency phase biases and satellite attitude files have been uploaded to the CNES website since June 4, 2019.



### Data description and process schemes

In the process of multi-frequency and multi-GNSS PPP, GFZ rapid orbit and clock products as well as CNES post-processed phase biases were used. We applied attitude quaternion elements from attitude files to obtain the same satellite attitude model as CNES network end. Considering that CNES did not estimate BeiDou GEO and BeiDou-3 satellite phase biases in 2019, these satellites were excluded from our experiment. The satellite PCO and phase center variation (PCV) corrections provided by ‘igs\_2084.atx’ were applied for GPS L1/L2, Galileo E1/E5a/E5b/E6 and BeiDou B1/B2/B3 frequencies. For the third GPS frequency (L5), the same PCO and PCV corrections for the second frequency (L2) are used (Li et al.

2018). Since receiver PCO and PCV corrections for Galileo and BeiDou were not available, we use GPS correction for Galileo and BeiDou signals during the experiment. In addition, for L5, E5b, E6, and B3 frequency observables, the receiver PCO and PCV corrections for the second frequency were used (Li et al. 2018, 2019).

The EWL and WL ambiguities were fixed by rounding averaged strategy with several epochs. After fixing EWL and WL ambiguities successfully, the optimal integer solution of N1 ambiguity can be searched using least squares ambiguity decorrelation adjustment (LAMBDA). The ratio threshold was set to 2.0 (Teunissen 1995; Geng et al. 2019). Instead of fixing full ambiguities, partial AR method was applied to find a subset of integers that can be fixed (Li et al. 2018). Standard deviation of ambiguities larger than 0.8 cycles, satellite elevations of less than 10°, or short tracking arcs (EWL, WL < 150 s and N1 < 180 s) were not attempted to fix. We keep float solutions for these low-quality ambiguities and try to fix a subset of high-quality ambiguities. To avoid negative effects from possible incorrectly fixed ambiguities in the last epoch, float solutions were introduced into the next update of the filter.

The positioning errors were defined as the difference between the PPP solution and the reference coordinate from IGS SINEX weekly solutions. As shown in Fig. 2, observation data from 34 Multi-GNSS Experiment (MGEX) stations were selected, and the detailed strategy for PPP is summarized in Table 1.

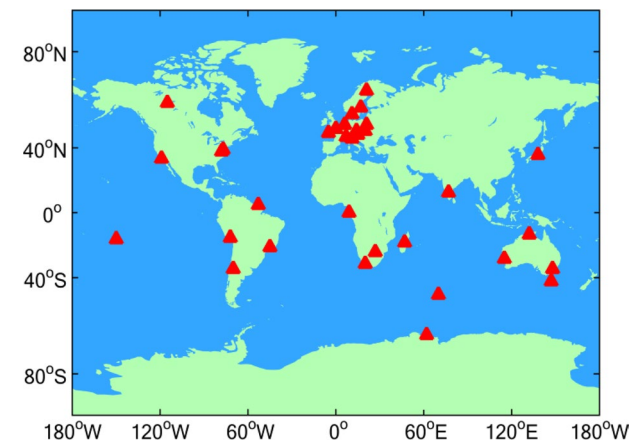


**Fig. 2** Distribution of the MGEX stations in this experiment. All these stations are equipped with Septentrio PolaRx5 and Trimble Alloy receivers, which are able to track GPS L1/L2/L5, Galileo E1/E5a/E5b/E6, and BeiDou B1/B2/B3 signals

### Impact of phase biases on the IFCBs

As a typical representative, time series for GPS L5, Galileo E5b and E6, BeiDou B3 phase biases in units of cycle on DOY 222, 2019 are shown in Fig. 3. The values of phase

**Table 1** Strategies for GPS/Galileo/BeiDou PPP

Item	Setting
Frequency	GPS L1/L2/L5; BeiDou B1/B2/B3; Galileo E1/E5a/E5b/E6
Orbits and clocks	GFZ rapid orbit and clock products
Code and phase biases	Post-processed code and phase biases from the CNES
Cutoff angle	10°
Sampling rate	30 s
Observation weighting	0.3 mm and 0.3 m for GPS/Galileo phase and pseudorange, 0.6 mm and 0.6 m for BeiDou phase and pseudorange (Li et al. 2017)
Phase wind-up	Phase polarization effects applied (Wu et al. 1993)
Satellite attitude	Applied the CNES satellite attitude
Zenith wet tropospheric delay	Estimated as a random walk ( $2.5 \times 10^{-11} m^2/s$ )
Ionosphere	Estimated as a random walk process ( $4 \times 10^{-6} m^2/s$ )
Station coordinate	Estimated as constant in static mode and white noise in kinematic mode
Phase ambiguities	N1 ambiguities were fixed by using LAMBDA, and the ratio threshold was set to 2.0 (Teunissen, 1995; Geng et al 2019)

**Fig. 3** Time series of phase biases on DOY 222, 2019. Different frequency types are shown in different panels. From left to right represents GPS L5, Galileo E5b, Galileo E6, and BeiDou B3, respectively

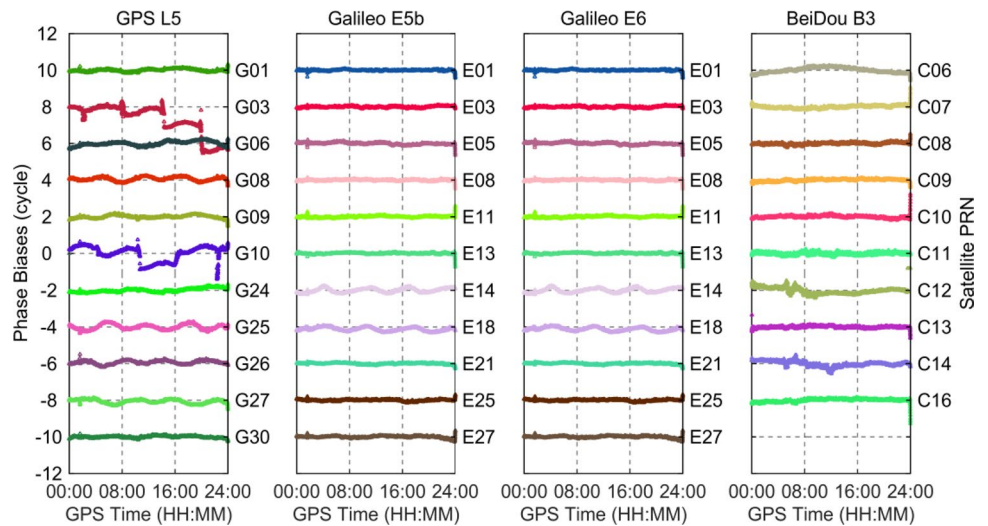
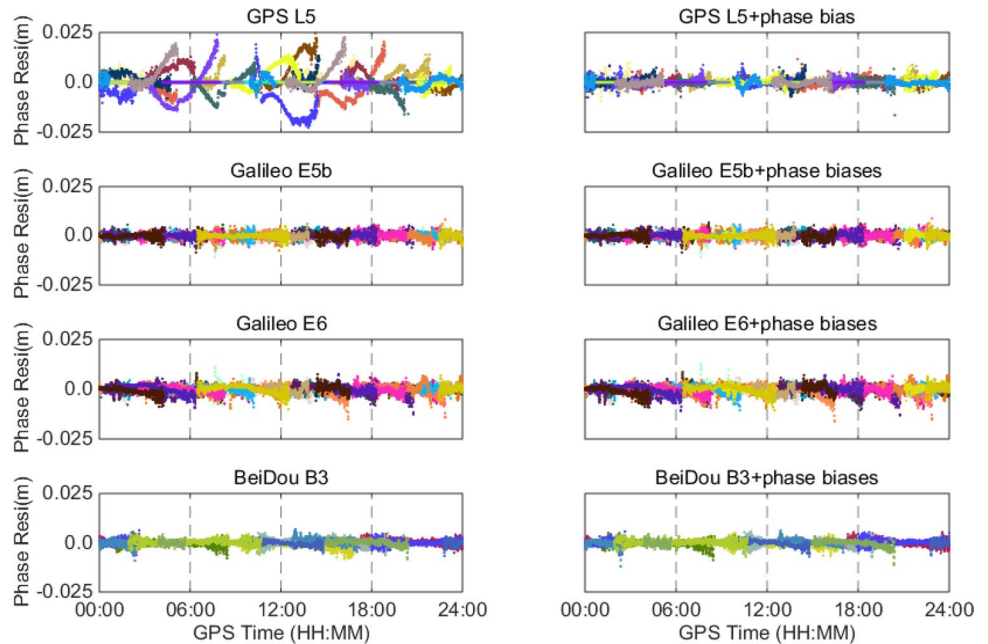


**Fig. 4** Residual carrier phase (left panels) and carrier phase + phase biases (right panels) for the KIRO station on DOY 222, 2019. Different satellites are identified by different colors



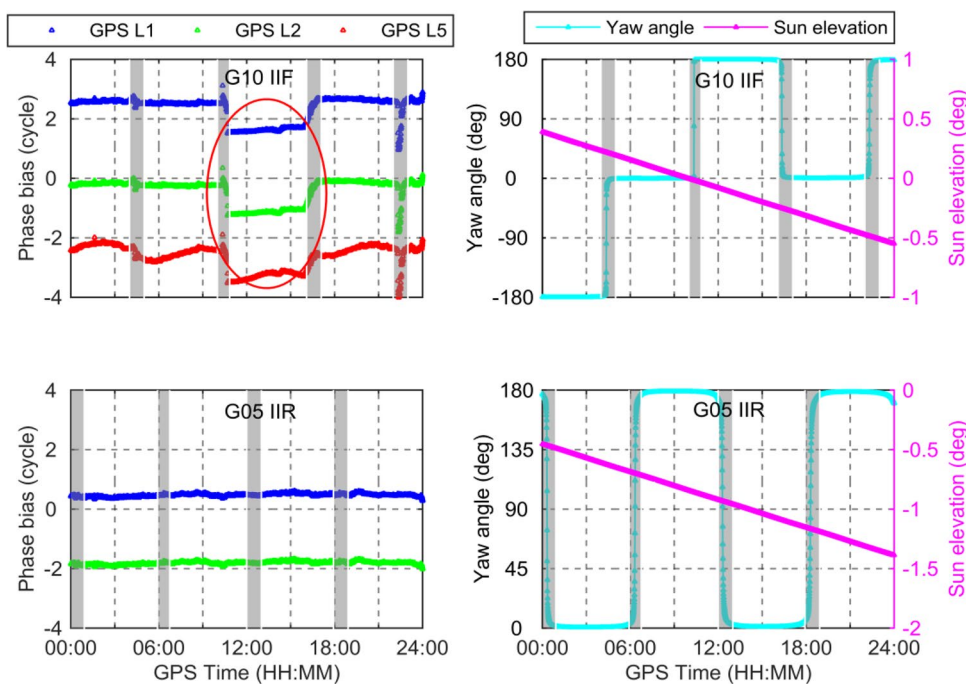
biases are offset for clarity purposes. As shown in (15), the time-dependent parts  $\delta b_{L5}^{G,s}$  of GPS L5 are absorbed into L5 phase biases, so it can be found that the periodic variations in the GPS IIF satellites and different amplitudes can be observed in different satellites. Following Montenbruck et al. (2012), the amplitude is related to sun elevation above the satellite orbital plane. On this day, the sun elevations for G03 and G10 are both approximately  $-0.1^\circ$ ; hence, the amplitudes of L5 phase biases for G03 and G10 are relatively larger than those of the other GPS IIF satellites. In addition, frequent jumps can be found for G03 and G10

phase biases. These are caused by the inconsistent satellite attitude  $yaw_{i,CNES-GFZ}$  between GFZ and CNES in the satellite maneuver periods, which will be proved in the following section. Variations in the phase biases for most Galileo satellites are stable except for E14 and E18, while the phase bias of Beidou shows poorer stability than that of Galileo.

Figure 4 shows the time series of the carrier phase residuals in GPS L5, Galileo E5b and E6, as well as BeiDou B3 at station KIRO on DOY 222, 2019. Large systematic errors of over 2.5 cm in the

GPS L5 carrier phase residual can be observed without phase biases. This phenomenon reflects the existence of

**Fig. 5** Time series of phase bias and yaw angle for the G10 Block IIF (top panels) and G05 Block IIR (bottom panels) satellites. The sun elevation variation is  $0.5^\circ$  to  $-0.5^\circ$  for G10 and  $-0.5^\circ$  to  $-1.5^\circ$  for G05. Gray bars indicate the satellite maneuver period



IFCBs in the GPS L5 observation carrier phase residuals. For comparison, the GPS L5 carrier phase residuals with phase biases are also presented in Fig. 4, and it is clear that the effect of IFCBs can be mitigated at the user end by using phase biases. For Galileo E5b and E6 together with BeiDou B3, we can see that the carrier phase residuals have almost no obvious systematic errors with these two methods.

### Impact of phase biases on the satellite maneuver period

Taking GPS as an example, the time series of phase biases, yaw angle, and sun elevation angle for G10 (Block IIF) and G05 (Block IIR) on DOY 222 and 2019 are shown in Fig. 5. The yaw angle is obtained by the satellite attitude file provided by the CNES, and the gray bars indicate the satellite maneuver period. From Fig. 5, we can see that the G10 IIF sun elevation angle is approximately  $0^\circ$ , and pronounced variations can be found for the G10 IIF L1, L2, and L5 phase biases in the maneuver periods, while no obvious variations can be found for the G05 IIR L1 and L2 phase biases. According to (15), the inconsistent yaw attitude errors  $yaw_{i,CNES-GFZ}$  between GFZ and CNES are absorbed into phase biases for each frequency. These also reflect that different attitude models of the GPS IIF satellites are applied between CNES phase biases and GFZ rapid orbit, clock products in the satellite maneuver periods.

In addition, a cycle bias of approximately 1.0 can be found in the red circle of Fig. 5. The reason for this 1.0 cycle bias is that the CNES and GFZ apply the reverse yaw direction for G10 at the low sun elevation (Dilssner et al. 2011; Kuang et al. 2017). For example, the yaw angle variation range for CNES is  $0^\circ$  to  $180^\circ$ , while it is  $0^\circ$  to  $-180^\circ$  for GFZ in the maneuver periods. Because of the reverse yaw direction, approximately 1.0 cycle wind-up errors are mostly absorbed into phase biases. Once introduced, a 1.0 cycle bias remains in the phase biases until the end of the orbit solution arc or the next reverse yaw direction occurs (Kuang et al. 2017). The impact of reverse yaw direction on the static and kinematic PPP accuracy will be investigated in the next section.

To verify the validity of phase biases and satellite attitude file in the maneuver periods, observation of station GRAZ and USN7 was selected. Figure 6 shows the G10 IIF and G05 IIR satellite carrier phase residuals by using the two different methods. It is obvious that large systematic errors of greater than 3 cm can be observed for the G10 IIF L1 carrier phase residual without phase biases. When phase biases are added to the raw measurement, the G10 IIF carrier phase residuals can be significantly reduced.

The ambiguity residual can be used as an integer property indicator for AR. In our experiment, observations of 34 MGEX stations were used to estimate the EWL, WL, and N1 ambiguities. By using phase biases and CNES satellite attitude, the estimated ambiguities of (17) are still contaminated by receiver hardware delay. To recover the integer property of ambiguity, we select the highest elevation of the satellite



**Fig. 6** Residuals of G10 IIF carrier phase (top panels) at station GRAZ station and G05 IIR carrier phase (bottom panels) at station USN7 on DOY 222, 2019. Gray bars indicate the satellite maneuver period

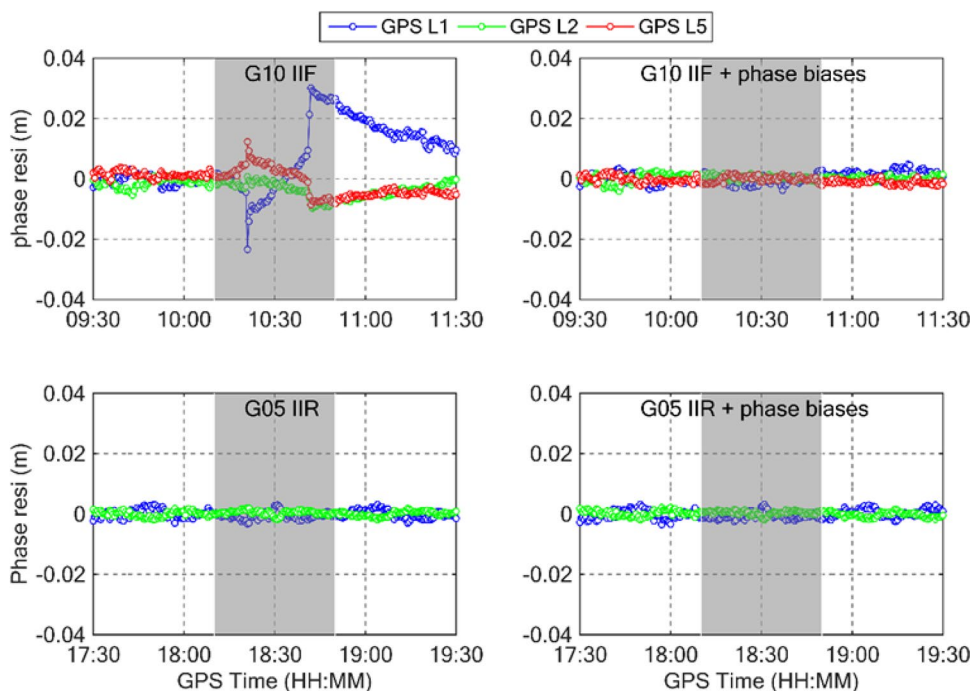


**Fig. 7** Residual distributions of the EWL (left panel), WL (middle panel), and N1 (right panel) ambiguity for G10 in the reverse yaw maneuver period

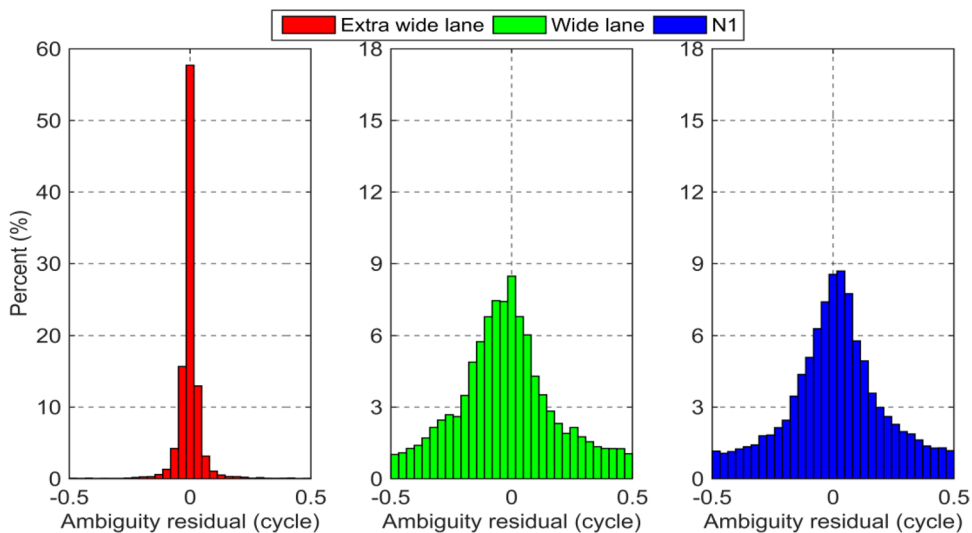


**Table 2** List of the data processing strategies

Strategy	Details	Ambiguity
No phase bias	Apply CNES satellite attitude without phase biases	Float
Delete	Delete satellites during the maneuver period	Float
With phase bias	Apply CNES satellite attitude with phase biases	Fixed

as a datum. The ambiguities with float values are rounded to their nearest integers in each epoch. Then, the ambiguity residuals can be expressed by the differences between the float values and their corresponding integer values of ambiguities. Figure 7 shows the ambiguity residual distributions

of G10 in the reverse yaw maneuver period (red circle of Fig. 5). It can be seen from this figure that the EWL, WL, and N1 ambiguity residuals follow standard normal distributions. Therefore, we conclude that the integer property of

**Table 3** Reverse yaw maneuvers of GPS, Galileo, and BeiDou between CNES and GFZ products

SYSTEM	PRN	DOY
GPS	G02, G21	168, 2019
	G06	170, 2019
	G01	171, 2019
	G12	201, 2019
	G16, G28	202, 2019
	G20	217, 2019
	G22	219, 2019
	G05	221, 2019
	G03, G10	222, 2019
	Galileo	E11, E12, E13, E33, E36
E01, E02, E21, E24, E25, E27, E30, E31		177, 2019
C13		163, 2019

ambiguity can be recovered by using phase biases and CNES satellite attitude in the reverse yaw maneuver period.

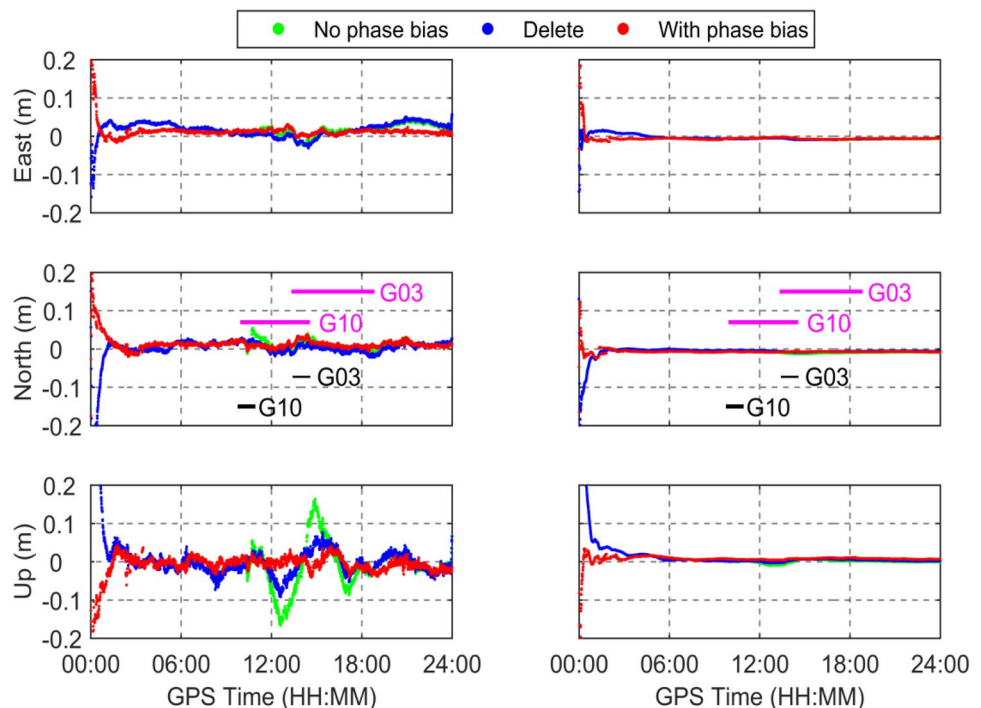
### Static and kinematic PPP AR in the reverse yaw maneuver period

To investigate the benefits from phase biases in the case of reverse yaw maneuvers, three data processing strategies are listed in Table 2. The first strategy (NO PHASE BIAS) uses CNES satellite attitude without phase biases, and second

strategy (DELETE) deletes the satellite data during maneuver periods. In both strategies, the ambiguities are kept float solutions. The third strategy (WITH PHASE BIAS) uses CNES satellite attitude with phase biases, and the ambiguities will be fixed. We collect information about the reverse yaw maneuver between CNES and GFZ from DOY 152 to 243, 2019, and these results are shown in Table 3.

We take station KIRO on DOY 222, 2019, as an example. The 1-day kinematic and static positioning errors for different PPP strategies are given in Fig. 8. We observe that the static and kinematic positioning errors in the east (E) direction can be reduced by AR. After filter convergence, the static positioning errors of different strategies are almost the same. However, the kinematic positioning errors of DELETE and NO PHASE BIAS strategies are obviously larger than those of the WITH PHASE BIAS strategy. In the up (U) direction, the NO PHASE BIAS strategy positioning errors can reach up to 15 cm. From Figs. 3 and 8, we notice that the maneuvering satellites including G03 and G10 and that these two satellites have reversed yaw directions during the maneuver periods. At the PPP user end, the reversed yaw direction would cause the approximately 1.0 cycle wind-up errors until the end of the observation arc or the next reverse yaw direction occurs. Therefore, these errors will continue to affect the positioning accuracy after the end of the maneuvering period, even if we delete this satellite during the maneuvering period. In kinematic PPP solutions, these errors will seriously damage the accuracy of epoch-dependent parameters such as station coordinates. As concluded in the above

**Fig. 8** Kinematic (left panels) and static (right panels) PPP for station KIRO on DOY 222, 2019, by using different strategies. Black lines represent the G03 and G10 satellite maneuver periods, while purple lines represent the G03 and G10 observation arcs for station KIRO



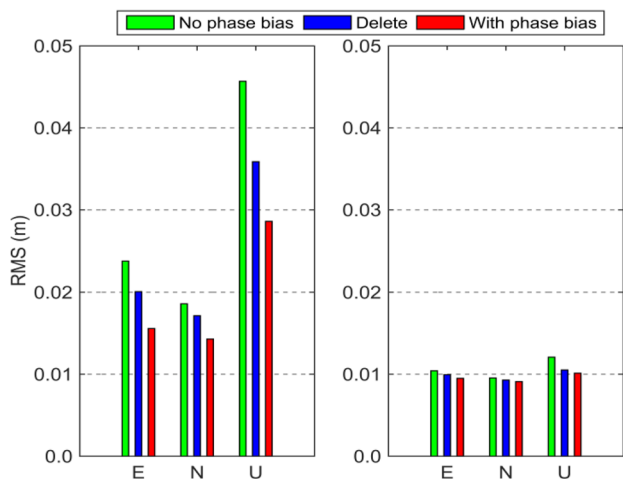


Fig. 9 RMS values in the E, N, and U directions in the kinematic (left panel) and static (right panel) PPP for different strategies

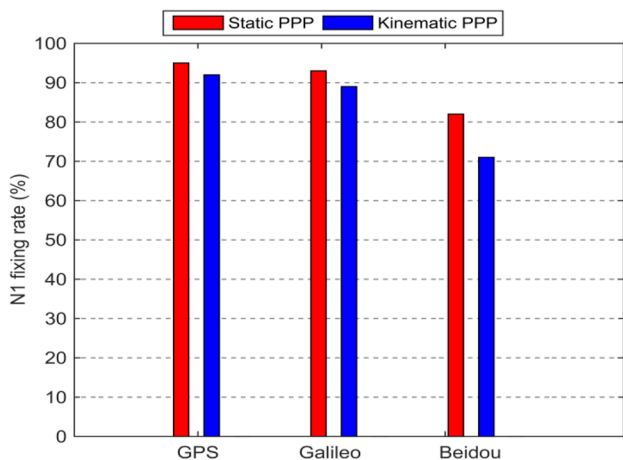


Fig. 10 Fixing rate of N1 ambiguities for the different systems in static and kinematic PPP AR

section, the 1.0 cycle wind-up errors are mostly absorbed into phase biases (Fig. 5); the influence of these errors on the PPP user end can be mitigated by using phase biases.

The 12-day (Table 3) datasets from 34 MGEX stations were employed for static and kinematic PPP accuracy analysis to further analyze the benefit of phase biases on reverse yaw maneuver. We calculated the root mean square (RMS) in E, north (N) and U directions, as shown in Fig. 9 for both static and kinematic PPP. We can see that three strategies show similar positioning performance in static PPP, and the positioning accuracy of WITH PHASE BIAS strategy can reach approximately 0.9, 0.8, and 1.0 cm in the E, N, U directions, respectively. In kinematic PPP, however, the RMSs of the three strategies are significantly different. Compared with NO PHASE BIAS strategy, the RMS of WITH PHASE BIAS strategy can be reduced by

34.4%, 23.1%, and 37.4% (from 2.38, 1.86, and 4.57 cm to 1.56, 1.43, and 2.86 cm) in the E, N, and U directions, respectively. These results indicate that the positioning performance can be improved by using the phase biases in the reverse yaw maneuver periods.

The N1 ambiguity fixing rate  $N_{1\_rate}$  is a useful indicator to assess the performance of PPP AR. It is calculated with the following formula:

$$N_{1\_rate} = \frac{N_{1\_fixed}}{N_{1\_total}} \times 100\% \tag{19}$$

where  $N_{1\_fixed}$  denotes the number of N1 ambiguities-fixed and  $N_{1\_total}$  denotes the number of total ambiguities-float. Figure 10 shows the fixing rate of GPS, Galileo, and BeiDou in static and kinematic PPP. The fixing rates of GPS are approximately 94.7% and 91.3% in static and kinematic modes, respectively, while Galileo shows almost the same fixing rate as GPS. Through comparing the fixing rate of GPS, Galileo, and BeiDou, it can be seen that fixing rate of GPS and Galileo is higher than that of BeiDou, which may be caused by the lower accuracy of BeiDou orbit and clock products (Steigenberger and Montenbruck 2019).

### Conclusion and summary

Multi-frequency and multi-GNSS PPP-AR with post-process phase biases and satellite attitude files are implemented by CNES, which are based on GFZ rapid orbit and clock products. By using these products, integer property of ambiguity can be recovered at the user end. In this paper, we introduced the transformation between phase biases and IRC model in the multi-frequency case. The theoretical derivation and experimental results demonstrate that GPS L5 IFCBs and inconsistent satellite attitude errors between CNES and GFZ products will be absorbed into the multi-frequency phase biases.

To assess the performance of phase biases in satellite maneuvers and low sun elevations, the phase residual and positioning performance of static and kinematic PPP AR were evaluated with 34 MGEX tracking stations. We find that through using these phase biases and satellite attitude files, the effect of IFCBs and inconsistent satellite attitude errors can be mitigated at the user end. Under the condition of satellite reverse yaw maneuver, the influence of reverse yaw maneuver on static PPP is not significant. However, the performance of kinematic PPP without phase biases or deleting maneuvering satellites will degrade significantly until the end of satellite observation arc or the next reverse yaw maneuver occurs. By applying phase biases with AR, the kinematic positioning accuracy can be improved by 34.4%, 23.1%, and 37.4% in the E, N, and U directions, respectively.

We conclude that the positioning accuracy, reliability, and availability performance can be improved by applying post-process phase biases with AR. When using GFZ rapid orbit and clock products, it is suggested that PPP users apply phase biases and satellite attitude files that are provided by CNES, especially for satellite maneuvers and low sun elevations.

**Acknowledgments** The authors gratefully acknowledge IGS MGEX for providing GNSS data. We also acknowledge the GFZ and CNES for providing precise products. This research was funded by Natural Science Innovation Group Foundation of China (No. 41721003), National Science Fund for Distinguished Young Scholars (No. 41525014), National Key Research and Development Program of China (2018YFC1503600), National Dam Safety Research Center (Grant No. CX2019B05), National Nature Science Foundation of China (No. 41704030), and Opening Foundation of Hunan Engineering and Research Center of Natural Resource Investigation and Monitoring (2020-4).

**Data Availability** The availability of multi-frequency phase biases and satellite attitude files is provided freely by CNES ([www.ppp-wizard.net/products/POST\\_PROCESSED](http://www.ppp-wizard.net/products/POST_PROCESSED)). The rapid orbit and clock products are provided freely by GFZ (<ftp://ftp.gfz-potsdam.de/pub/GNSS/products/mgnss>). GNSS data, IGS SINEX weekly solutions files, and `igs_2084.atx` files are provided freely by IGS and MGEX (<https://cddis.nasa.gov/archive/gps/data/daily>).

## References

- Banville S, Geng J, Loyer S, Schaer S, Springer T, Strasser S (2020) On the interoperability of IGS products for precise point positioning with ambiguity resolution. *J Geod* 94(10):1–15
- Cao X, Li J, Zhang S, Kuang K, Gao K, Zhao Q, Hu H (2018) Uncombined precise point positioning with triple-frequency GNSS signals. *Adv Space Res* 63(9):2745–2756
- Collins P, Lahaye F, Herous P, Bisnath S (2008) Precise point positioning with ambiguity resolution using the decoupled clock model. In: Proceedings of ION GNSS 2008, Institute of Navigation, Savannah, Georgia, 16–19 September, pp 1315–1322
- Dilssner F, Springer T, Enderle W (2011) GPS IIF yaw attitude control during eclipse season, AGU Fall Meeting, San Francisco, Dec 9, [http://acc.igs.org/orbits/yaw-IIF\\_ESOC\\_agu11.pdf](http://acc.igs.org/orbits/yaw-IIF_ESOC_agu11.pdf)
- Ge M, Gendt G, Rothacher M, Shi C, Liu J (2008) Resolution of GPS carrier-phase ambiguities in Precise Point Positioning (PPP) with daily observations. *J Geod* 82(7):389–399
- Geng J, Meng X, Dodson A, Teferle F (2010) Integer ambiguity resolution in precise point positioning: method comparison. *J Geod* 84(9):569–581
- Geng J, Guo J, Chang H, Li X (2019) Toward global instantaneous decimeter-level positioning using tightly coupled multi-constellation and multi-frequency GNSS. *J Geod* 93:977–991. <https://doi.org/10.1007/s00190-018-1219-y>
- Guo J, Geng J (2018) GPS satellite clock determination in case of inter-frequency clock biases for triple-frequency precise point positioning. *J Geod* 92(10):1133–1142
- Kouba J (2009) A simplified yaw-attitude model for eclipsing GPS satellites. *GPS Solut* 13(1):1–12
- Kouba J, Héroux P (2001) Precise point positioning using IGS orbit and clock products. *GPS Solut* 5(2):12–28
- Kuang D, Desai S, Sibois A (2017) Observed features of GPS Block IIF satellite yaw maneuver and corresponding modeling. *GPS Solut* 21(2):739–745
- Laurichesse D, Mercier F (2009) Integer ambiguity resolution on undifferenced GPS phase measurements and its application to PPP and satellite precise orbit determination. *Navig J Inst Navig* 56(2):135–149
- Laurichesse D, Privat A (2015) An open-source PPP client implementation for the CNES PPP-WIZARD demonstrator. In: Proceedings ION GNSS 2015, Institute of Navigation, Tampa, USA, September 14–18, pp 2780–2789
- Li P, Zhang X, Ren X, Zuo X, Pan Y (2016) Generating GPS satellite fractional cycle bias for ambiguity-fixed precise point positioning. *GPS Solut* 20(4):771–782
- Li P, Zhang X, Guo F (2017) Ambiguity resolved precise point positioning with GPS and BeiDou. *J Geod* 91(1):25–40
- Li P, Zhang X, Ge M, Schuh H (2018) Three-frequency bds precise point positioning ambiguity resolution based on raw observables. *J Geod* 92(12):1357–1369
- Li X, Li X, Liu G, Feng G, Yuan Y, Zhang K, Ren X (2019) Triple-frequency PPP ambiguity resolution with multi-constellation GNSS: BDS and Galileo. *J Geod* 93(3):1105–1122
- Liu X, Jiang W, Li Z, Chen H, Zhao W (2019) An analysis of inter-system biases in BDS/GPS precise point positioning. *GPS Solut* 23(4):1–14
- Liu T, Jiang W, Laurichesse D, Chen H, Liu X, Wang J (2020) Assessing GPS/Galileo real-time precise point positioning with ambiguity resolution based on phase biases from CNES. *Adv Space Res* 66(4):810–825
- Lou Y, Zheng F, Gu S, Liu Y (2015) The impact of non-nominal yaw attitudes of GPS Satellites on Kinematic PPP Solutions and their Mitigation Strategies. *J Navigation* 68(4):1–17
- Loyer S, Banville S, Perosanz F, Mercier F (2017) Disseminating GNSS satellite attitude for improved clock correction consistency. Poster presented at the 2017 IGS Workshop, Paris
- Malys S, Jensen PA (1990) Geodetic point positioning with GPS carrier beat phase data from the CASA UNO experiment. *Geophys Res Lett* 17(5):634–654
- Montenbruck O, Hugentobler U, Dach R, Steigenberger P, Hauschild A (2012) Apparent clock variations of the Block IIF-1 (SVN62) GPS satellite. *GPS Solut* 16(3):303–313
- Montenbruck O, Steigenberger P, Prange L, Deng Z, Zhao Q, Perosanz F, Romero I, Noll C, Stuerze A, Weber G, Schmid R, Macleod K, Schaer S (2017) The Multi-GNSS Experiment (MGEX) of the International GNSS Service (IGS)-achievements, prospects and challenges. *Adv Space Res* 59(7):1671–1697
- Pan L, Zhang X, Li X (2017) Characteristics of inter-frequency clock bias for Block IIF satellites and its effect on triple-frequency GPS precise point positioning. *GPS Solut* 21(2):811–822
- Schaer S (2016) Bias-SINEX format and implications for IGS bias products. IGS Workshop. Australia, February, Sydney, pp 8–12
- Shi J, Gao Y (2014) A comparison of three PPP integer ambiguity resolution methods. *GPS Solut* 18(4):349–528
- Steigenberger P, Montenbruck O (2019) Consistency of MGEX Orbit and Clock Products. *Engineering*. <https://doi.org/10.1016/j.eng.2019.12.005>
- Teunissen P (1995) The least-squares ambiguity decorrelation adjustment: a method for fast GPS integer ambiguity estimation. *J Geod* 70(1–2):65–82
- Wang C, Guo J, Zhao Q, Liu J (2018) Yaw attitude modeling for BeiDou I06 and BeiDou-3 satellites. *GPS Solut* 22(4):1–10
- Wu J, Wu S (1993) Effects of antenna orientation on GPS carrier phase. *Manuscripta Geod* 18(2):91–98



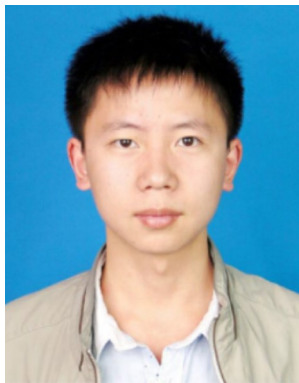
Xia F, Ye S, Chen D, Jiang N (2019) Observation of BDS-2 IGSO/MEOs yaw-attitude behavior during eclipse seasons. *GPS Solut* 23(3):23–71

Zhang X, Li P (2016) Benefits of the third frequency signal on cycle slip correction. *GPS Solut* 20(3):434–460

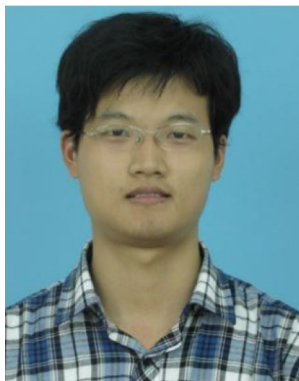
Zhou F, Dong D, Li P, Li X, Schuh H (2019) Influence of stochastic modeling for inter-system biases on multi-GNSS undifferenced and uncombined precise point positioning. *GPS Solut*. <https://doi.org/10.1007/s10291-019-0852-0>

Zumberge JF, Heflin MB, Jefferson DC, Watkins MM, Webb FH (1997) Precise point positioning for the efficient and robust analysis of GPS data from large networks. *J Geophys Res* 102(B3):5005–5017

**Publisher's Note** Springer Nature remains neutral with regard to jurisdictional claims in published maps and institutional affiliations.



**Tianjun Liu** received a BSc degree in 2016 from Anhui University of Science and Technology and a Master degree from China University of Mining and Technology in 2019 and is currently a PhD candidate in GNSS Research Center, Wuhan University. His current research mainly focuses on multi-GNSS precise positioning.



**Hua Chen** is currently a lecturer at Wuhan University. He obtained his BSc, Master, and PhD degrees with distinction in Geodesy and Engineering Surveying at the School of Geodesy and Geomatics in Wuhan University in 2009, 2011, and 2015. His main research interests include GNSS data processing of large-scale networks, GNSS orbit determination, and clock estimation research.



**Qusen Chen** got his PhD degree in 2018 from the School of Geodesy and Geomatics of Wuhan University. Now he is a postdoctoral fellow in the GNSS Research Center of Wuhan University, and his current research focuses on GNSS precise data processing and its application in deformation monitoring.



**Weiping Jiang** is currently a professor at the Wuhan University. He obtained his BSc, Master, and PhD degrees with distinction in Geodesy and Engineering Surveying at the School of Geodesy and Geomatics in Wuhan University in 1995, 1997, and 2001. His main research interests include GNSS data processing of large-scale networks, GNSS coordinate time-series analysis, satellite altimetry, and geodynamics research.



**Denis Laurichesse** received his engineering degree and an advanced study diploma (D.E.A.) from I.N.S.A. (National Institute for Applied Sciences), in 1988, in Toulouse, France. He worked at C.N.E.S (The French Space Agency) since 1992 and specializes in satellite precise orbit determination, navigation, and GNSS-based systems. He was the recipient of the ION Burka award in 2009 and the GPS World leadership award in 2019 for his work on phase ambiguity resolution.



**Xiangdong An** received his PhD in GNSS Research Center from Wuhan University in 2019. He received BSc degree in geomatics from Chang'an University in 2013. His main interests are GLONASS ambiguity resolution and inter-frequency bias determination.



**Tao Geng** is an associate professor at GNSS Research Center, Wuhan University, China. He received his PhD in Geodesy and Surveying Engineering from Wuhan University in 2009. From February 2013 to February 2014, he was a visiting scholar at Ohio State University. His research interest focuses on precise GNSS orbit determination and positioning.